Coarse-Grained Simulations of Model Polymer Nanofibres[a]

Alberto Milani, Mosè Casalegno, Chiara Castiglioni, Guido Raos*

We describe the development of a coarse-grained (CG) force field for nylon-6 (polycaprolactam) and its application to the simulation of the structure and macromolecular dynamics within cylindrical fibres formed by this polymer, having diameters in the 14–28 nm range. Our CG model is based on the MARTINI force field for the non-bonded interactions and on Boltzmann-inverted gas-phase atomistic simulations for intramolecular stretching and bending energies. The simulations are carried out on infinite, isolated nanofibres at temperatures of 300, 400 and 500 K, with different starting configurations. Starting from ordered chain-extended configurations, we simulate the melting of the polymer in the nanofibres and, after cooling back to room temperature, its re-crystallization in a chain-folded lamellar configuration. This agrees with experimental observations on electrospun nylon-6 nanofibres and demonstrated the suitability of the approach for the simulation of these systems. The effect of nanoscale confinement on the structure and dynamics of the polymer chains is extensively discussed.

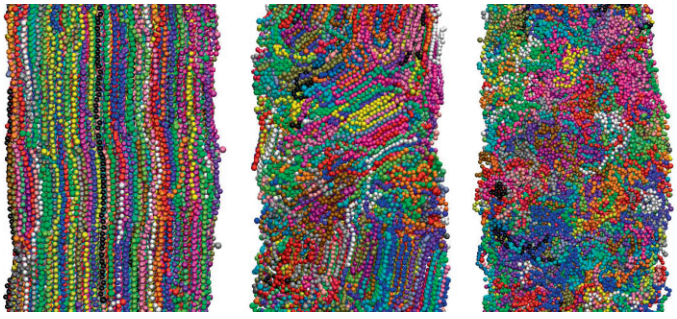

Introduction

From a broad and fundamental point of view, a major portion of nanotechnology research is about discovering ways of controlling the structure of materials at length scales which are intermediate between the molecular one, which is the traditional domain of chemistry, and the macroscopic one, which belongs to materials engineering. At the same time, we would like to learn about the ways in which the properties of materials deviate from bulk-like behaviour on decreasing their 'characteristic length scale' (whatever this means) down to 100 nm or less. Many intriguing phenomena (e.g., on polymer-based nanocomposites[1–7]) are still lacking a fully satisfactory interpretation, but there is widespread agreement that they can be largely ascribed to the increasing importance of interfacial phenomena on going down from micro- to nano-structured materials.

The electrospinning technique has been shown to provide a simple and quite general route to the production of nanostructured polymeric materials.[8–10] Under the 'right' operating conditions (solution concentration, rate of extrusion, strength of applied field, etc.), it is possible to produce long continuous filaments with diameters of $\cong 10^1$ nm, so that one can rightly speak of nanofibres in this case. Many different types of polymers have been successfully electrospun, after a due amount of trial-and-error to find the optimal processing conditions. The nanofibres can be also functionalized, by adding different types of

A. Milani, M. Casalegno, C. Castiglioni, G. Raos
Dipartimento di Chimica, Materiali e Ingegneria Chimica "G. Natta", Politecnico di Milano, via L. Mancinelli 7, 20131 Milano, Italy
Fax: +39-02-2399-3080; E-mail: guido.raos@polimi.it

[a] **Supporting Information** for this article is available from the Wiley Online Library or from the author.

DOI: 10.1002/mats.201100010

molecules to the solution before spinning (e.g., dyes, surfactants, biomolecules, nanoparticles, etc.). It is not surprising that usage of electrospun nanofibres has been envisaged in quite disparate fields, such as template materials synthesis, catalysis, active filtering, nanocomposites, cell growth, tissue engineering and controlled drug release.

There is currently a lot of interest in gathering information about the structure and properties of electrospun polymer materials, such as the average chain conformation, their degree of orientational order and (if applicable) the type and amount of crystallinity. In thin nanofibres, these are expected to be strongly affected by the presence of an extended interface. Due to large elongational stresses and the rapid solvent evaporation during the spinning process, their structure may often correspond to some 'frozen' non-equilibrium state. The classic polymer characterization techniques (microscopies, spectroscopic and scattering methods, calorimetry, etc.) can be used to study these materials, but the interpretation of the data is often far from straightforward. In addition, these methods often lack the spatial resolution necessary to investigate the properties of individual nanofibres (an interesting exception is represented by AFM, which has been adapted to measure the elongational modulus of single nanofibres[11]).

Computer simulations have been increasingly used alongside experimental measurements in the investigation of the structure and properties of virtually all polymeric systems. In the specific context of the present paper, we are aware of a few simulation studies of polyethylene (PE) nanofibres, respectively, using the Monte Carlo (MC)[12] and the Molecular Dynamics (MD)[13] methods. Mattice and co-workers[12] simulated chains of 50 beads on a high coordination lattice. Each bead represents two consecutive methylene groups. Their first two papers concerned molten PE fibres at 509 K (236 °C), respectively, looking at spatially resolved structural properties[12a] (showing for example that the chain ends tend to segregate at the fibre surface) and some global dynamical properties[12b] (showing an enhanced chain mobility, compared to the bulk polymer under comparable conditions). In their third paper,[12c] they studied the crystallization behaviour after quenching these nanofibres to room temperature. The chains tended to adopt an extended conformation, parallel to the fibre axis. Crystallization started at the surface and propagated towards the interior, leaving a somewhat disordered core inside the fibre.

Rutledge and co-workers[13] simulated a united-atom PE model, consisting of chains of 50–300 carbon atoms. In a first paper,[13a] they simulated the structure and interfacial properties of fibres with diameters in the 2–23 nm range. The systems were equilibrated at 495 K (222 °C), and then cooled down to 100 K to study the size-dependence of the polymer glass transition temperature. The fast cooling rate adopted in the simulations did not allow any crystallization of the polymer. The significant depression of the observed T_g (100 °C below the bulk value for the thinnest fibres, under otherwise comparable simulation conditions) was correlated with the finite thickness of the interfacial layer, where the polymer chains enjoy greater mobility. This size-dependence of the glass transition temperature has been seen also experimentally, on several related system (e.g., confined or free-standing polymer thin films).[5,14] In a subsequent paper,[13b] the same group simulated the tensile properties of these model nanofibres, observing a decrease of the Young modulus and of the plastic yield stress on going to thinner and thinner fibres.

In this contribution, we shall describe MD simulations of model polycaprolactam (polyamide-6 or nylon-6, henceforth NY6) nanofibres. Several groups have applied the electrospinning technique to this polymer[15] and to its nanocomposites incorporating clay platelets.[16] In the newly formed nanofibres, the chains tend to crystallize in the metastable γ-form and are preferentially oriented along the fibre axis.[15a] Following melting and annealing at 100 °C, the polymer re-crystallizes in the thermodynamically stable α-form and the average orientation of the chains changes from longitudinal to orthogonal with respect to the fibre axis.[15b] The tensile properties of single, as-prepared NY6 nanofibres have also been measured by AFM.[16a] It was found that the smaller fibres had a higher Young modulus, going from 20 to 30 MPa on decreasing the diameter from 120 to 80 nm. These peculiar structural properties of polyamide nanofibres and their evolution as a function of external variables still need to be explained. Computational studies such as the present one are highly desirable, to confirm and interpret the trends observed experimentally.

Atomistic MD simulations of polymer nanofibres would require enormous amounts of computational resources, if one really wanted to approach experimentally significant systems (with respect to polymer molecular weight, fibre diameter, annealing conditions, etc.). In addition, in the particular case of NY6, there are still unresolved issues concerning the precise crystal structure of its polymorphs (α, γ, δ and their variants with various degrees of disorder) and the phase transitions between them: see ref.[17] for experimental studies (largely based on X-ray diffraction data) and ref.[18] for recent molecular modelling work (by molecular mechanics energy minimizations). For both of these reasons, we judged that it would have been premature to attempt atomistic MD simulations and decided to adopt a coarse-grained (CG) model of NY6. Several alternative methods have been proposed to carry out such coarse-graining in an accurate and systematic way.[19] Typically, these are geared towards the description of amorphous phases (liquids and glasses). Müller-Plathe and coworkers have recently developed a CG model of a

related polymer, namely nylon-6,6 (NY66),[20] by 'Iterative Boltzmann Inversion'[19b] of atomistic MD simulations. This method reproduces the key structural properties of the bulk polymer liquid (pair distribution functions) and yields the CG interaction potentials in numerical form. Instead, we adopted a much simpler approach and based our model on the MARTINI force field by Marrink and co-workers.[21] This choice was determined by the extreme simplicity of this method, especially compared to other approaches,[19] but also by our future plans to simulate the interaction of these nanofibres with other materials, such as aqueous polypeptides and proteins (important for cell growth and tissue engineering). From our point of view, the fact that these materials have already been parametrized within MARTINI represents a major point in favour of this particular CG paradigm.

In the following Section, we will provide details about our CG parametrization and our simulation protocols. The latter turn out to be quite important since, in analogy with many experimental observations on electrospun nanofibres, our simulation results are strongly dependent on the initial preparation and history of the samples. The resulting structural and dynamical properties of the polymer nanofibres will be described in Results and Discussion, demonstrating the suitability of this CG approach in describing structural transitions as a function of temperature, in agreement with experimental observations.[15,16]

Simulation Details

Model and Parametrization

CG simulations of NY6 nanofibres were carried out and post-processed by means of the GROMACS 4 package.[22] As illustrated in Figure 1, we represent NY6 as an alternating copolymer consisting of apolar and polar spherical beads, respectively, representing the $-(CH_2)_4-$ and the $-CO-NH-CH_2-$ units. We used the MARTINI force field[21] for the description of all intra- and intermolecular non-bonding interactions. This force field was originally developed for the purpose of carrying out fast, semi-quantitative simulations of large ensembles of biological molecules, such as lipids,[21a] proteins,[21b] carbohydrates[21c] and their supramolecular assemblies (e.g., cell membranes). Recently it has also been extended to some synthetic polymers, namely poly(ethylene oxide) (PEO)[21d] and polystyrene (PS).[21e] Notice that the $-(CH_2)_4-$ unit is present in saturated lipid chains, whereas the $-CO-NH-CH_2-$ unit is typical of proteins (in fact, it corresponds to glycine). Therefore, parameters for these units already been developed and thoroughly tested within MARTINI.

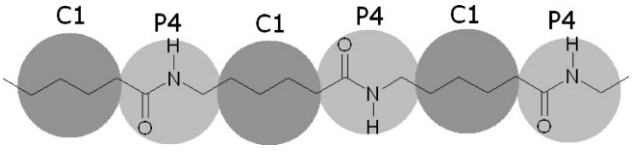

Figure 1. Molecular structure of nylon-6 and its mapping onto the coarse-grained model.

One key aspect of the MARTINI approach is that it adopts the Lennard-Jones (LJ) function to represent the non-bonded interactions between the CG beads (if the beads had a non-zero net charge, there would be in addition a Coulomb interaction term):

$$V_{n.b.} = \sum_{i<j} V_{ij}^{\mathrm{LJ}}(r_{ij}) = \sum_{i<j} \left\{ 4\varepsilon_{ij} \left[\left(\frac{r_{ij}}{\sigma}\right)^{12} - \left(\frac{r_{ij}}{\sigma}\right)^{6} \right] - V_{\mathrm{cut}} \right\}, \quad (1)$$

where r_{ij} is the interparticle distance. These interactions are computed among all pairs of beads within the cutoff distance r_{cut} 1.2 nm, including also second and third nearest-neighbours along the polymer chain (1–3 and 1–4 interactions). V_{cut} is a constant, chosen so that the potential energy is continuous (i.e., exactly zero) at the cutoff. In MARTINI, all normal particle types have the same LJ diameter $\sigma = 0.47$ nm, while the LJ well depths (ε_{ij}) are adjusted so as to reproduce a large set of experimental thermodynamic data (e.g., oil–water partition coefficients for several simple molecules). Following MARTINI's notation, we assigned particle type P4 to the polar fragments, and particle type C1 to the apolar ones.[23] This implies the following interactions energies, in $\mathrm{kJ \cdot mol^{-1}}$: 3.5 (C1. . .C1), 5.0 (P4. . .P4) and 2.0 (P4. . .C1). Note that the 'cross' interaction falls outside the boundaries set by the two 'diagonal' ones and it cannot be justified by any kind of average or combination rule, such as those which are frequently adopted by atomistic force fields.[24] This depends on the fact that we are now dealing with CG interactions, which in general result from a sum of contrasting physical effects.

The intramolecular part of our CG force field consists of bond stretching and bond angle bending terms. The MARTINI force field comes with a standard set of analytical potentials and parameters, which, however, depend on the *a priori* assignment of specific conformations or secondary structure motifs ('helix', 'coil', 'extended', 'turn' or 'bend', in the case of proteins[21b]). Instead of choosing a specific set of potential functions, we decided to follow a slightly more general approach and adapt the MARTINI force field to the NY6 polymer. To this aim, we generated our stretching and bending potentials by Boltzmann inversion of an all-atom simulation of a short NY6 chain, consisting of six monomer units with two *n*-butyl end groups. Considering our initial aim to develop a semi-quantitative description of NY6, the

resulting potentials are perhaps 'more detailed than necessary', but this does not represent a real disadvantage of our approach.

We used the Tinker 4.2 package[25] and the OPLS-AA force field[26] to conduct a room-temperature (298 K) stochastic dynamics simulation of the NY6 oligomer, in the gas phase.[27] In this atomistic simulation, the atomic friction coefficient was set to the default value $\zeta = 91.0\ \mathrm{ps}^{-1}$ and the time step was $\Delta t = 2$ fs, using bond constraints to avoid the fast vibrations of the H atoms. We collected 10^5 independent configurations within a total simulation time of 10 ns (a reviewer suggested to check this using a longer simulation: plots of the distributions obtained from one 30 ns run are given in the Supporting Information). From each frame of this simulation, we calculated the bond length and bond angle distributions between the centres-of-mass of the CG units ($W_{\mathrm{stretch}}(r)$ and $W_{\mathrm{bend}}(\theta)$, respectively). The terminal groups were excluded from this analysis. Following MARTINI's general philosophy of 'maximum simplicity', we decided to lump together the C1–P4–C1 and P4–C1–P4 bond angle distributions, to give a single average bending potential (plots of the two individual distributions are given in Figure S1, Supporting Information). Finally, the Boltzmann inversion was applied to these distributions to obtain the potentials:

$$\begin{aligned} V_{\mathrm{stretch}}(r) &= -RT\ln\left[W_{\mathrm{stretch}}(r)/r^2\right] + C \\ V_{\mathrm{bend}}(\theta) &= -RT\ln[W_{\mathrm{bend}}(\theta)/\sin(\theta)] - V_{13}^{\mathrm{LJ}}\left(2r_{\mathrm{eq}}\cos\theta\right) + C' \end{aligned} \tag{2}$$

where R is the gas constant. C and C' are constants, such that these stretching and bending potential functions take the value of zero at their absolute minimum (r_{eq} and θ_{eq}). V_{13}^{LJ} is the average LJ interaction energy between second nearest-neighbours along the NY6 chain. These 1–3 interactions must be subtracted from the bending potentials, since these are computed separately as part of the non-bonded energy (see above). Since these comprise both C1...C1 and P4...P4 interactions, we computed V_{13}^{LJ} by averaging the LJ parameters associated with them ($\varepsilon_{ij} = (5.0 + 3.5)/2 = 4.25\ \mathrm{kJ \cdot mol^{-1}}$). The resulting potential functions were tabulated in numerical form so as to be used within GROMACS. They are plotted in Figure 2 (lower panel).

As a final step in our CG parametrization, we tested the reliability of our Boltzmann-inverted potentials by carrying out another stochastic dynamics simulation of the same oligomer under identical conditions, but this time with the CG force field. The bond length and bond angle distributions were calculated again and compared to those from the all-atoms simulation. The results are shown in Figure 2 (upper panel) and they appear to be satisfactory.

The current CG force field, although explicitly parametrized with NY6 in mind, can only be expected to provide a semiquantitative description of its structure and properties. This is in line with MARTINI's philosophy of privileging simplicity over quantitative accuracy, thermodynamics over specific structural and dynamical quantities. This is confirmed by the comparison of our CG results with a few experimental data (bulk polymer densities and characteristic ratio), which will be discussed in the Results and Discussion section. The 'minuses', which in our opinion do not outweigh the 'pluses' deriving from the use of a simple and transferable CG approach, mainly depend on the lack of directionality of the hydrogen bonds and of the chain as a whole. As to the first point, we notice that MARTINI has been explicitly developed for proteins[21b] and polysaccharides,[21c] where hydrogen bonding interactions are notoriously important. In any case, there is no directionality also in other, much more sophisticated CG descriptions of hydrogen-bonded systems, such as the water and methanol models by Izvekov and Voth[19d] and the NY66 model by Müller-Plathe and coworkers,[20] where the atoms directly involved in the hydrogen bonds are lumped together within CG beads interacting by spherically symmetric potentials. As to the second point, we observe that the NY6 chain has no directionality in the CG representation, unlike the atomistic chain which has a well-defined one originating from the peptide bonds.[28] This directionality is important in the solid state, since the various crystal forms of NY6 (α, γ and δ) differ also by their hydrogen bond patterns, involving parallel iso- or anti-directional chains.[17,18] Unlike the NY6 crystallites obtained after long thermal annealing, those within the electrospun nanofibres will certainly incorporate (for kinetic reasons) a lot of up-down disorder. Therefore, because of the averaging produced by this disorder, here chain directionality might not be so important after all. In any case, we stress that we cannot expect our force field to reproduce the details of any of those NY6 crystal polymorphs.

Systems and Procedures

We simulated NY6 nanofibres with initial radii of 7, 10 and 14 nm. In the following, these systems will be denoted R7, R10 and R14. The nanofibres have infinite length and they are oriented along the *z*-axis. We adopted full three-dimensional periodic boundary conditions (PBC's). The *z* box size, corresponding to the nanofibre periodicity, was set equal to 32.54 nm (see also below). Since we were interested in simulating isolated nanofibres in vacuo, we excluded all fibre–fibre interactions by fixing the *x* and *y* box dimensions at 40 nm, for all the systems. Note that the fibre length/radius ratio is always less than 2π,[13] so as to avoid Rayleigh instabilities (see below). While the nanofibres are effectively infinite, the individual polymer chains have a finite

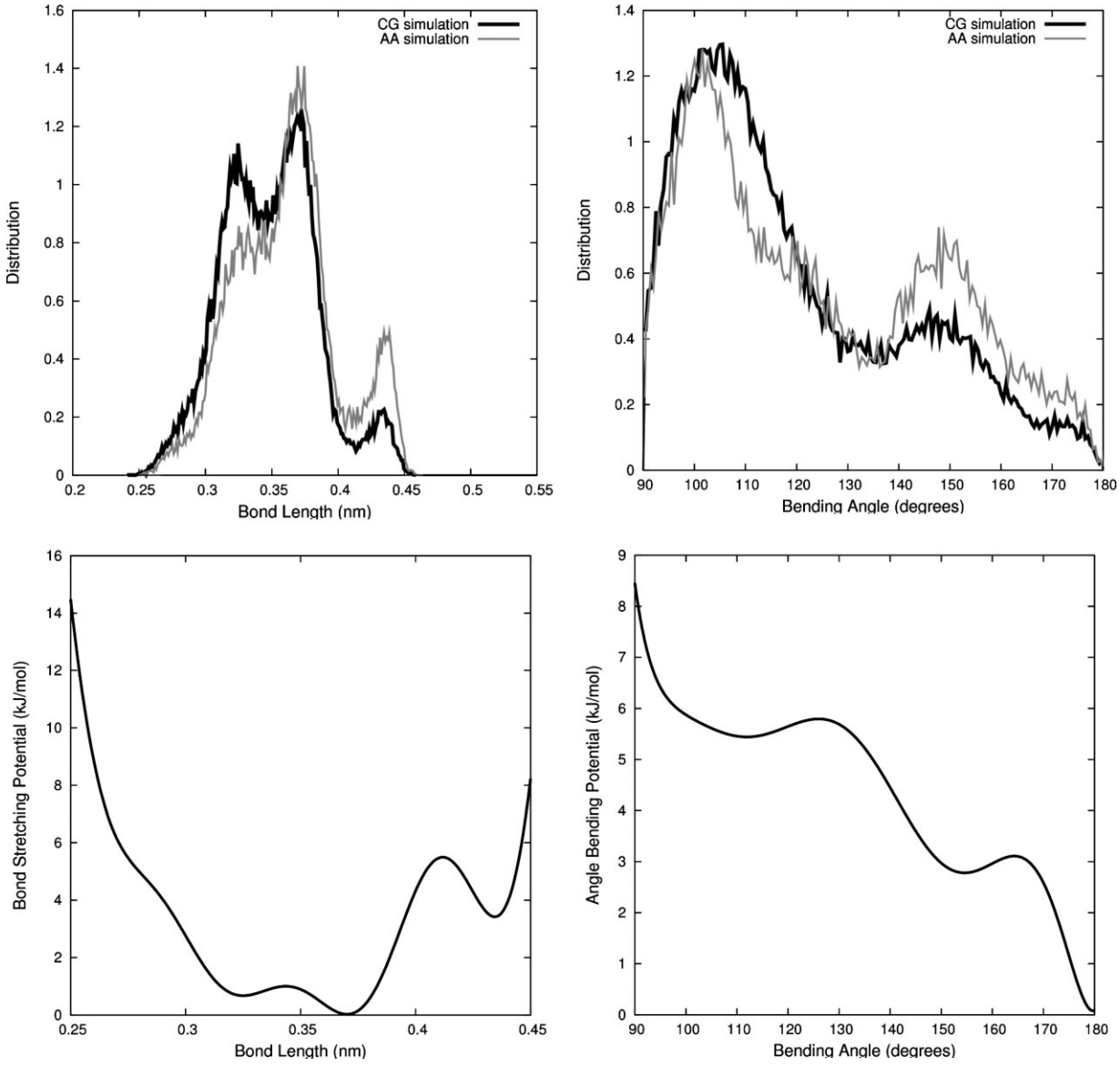

Figure 2. Top: distribution of the bond lengths (P4–C1) and bond angles (C1–P4–C1 and P4–C1–P4), from atomistic (grey) and coarse-grained (black) gas-phase simulations at 300 K. Bottom: effective coarse-grained potentials for bond stretching and bond angle bending. In the case of the bending potential in the figure we show the resulting potential after subtracting V_{13}^{U} interactions.

length. Their CG structure is C1–(P4–C1)$_{45}$ (overall, 91 CG beads, with two apolar ends). In an atomistic model, this would correspond to a molar mass $M = 5\,150\,\mathrm{g \cdot mol^{-1}}$.

Special care was taken in the definition of the starting configurations, since the results of any nanofibre MD simulation are expected to depend strongly on this choice. This problem does not simply arise from the limited time- and length-scales that can currently be explored by the MD method, with either all-atom or CG force fields. Instead, it reflects the experimental observation that the nanofibres may have quite different non-equilibrium structures, depending on the electrospinning conditions.[29] Therefore, similarly to previous work on PE nanofibres,[12,13] some of our simulations were started from amorphous polymer nanofibres equilibrated at 500 K. In addition, guided by some experimental results on NY6,[15] another set of simulations was started from a markedly anisotropic configuration, characterized by a strong chain stretching along the fibre axis.

Figure 3 shows two views of this ordered starting configuration for the R10 fibre. The chains are fully extended chains along the fibre axis, with a bond length of 0.356 nm. The *z*-axis periodicity of the fibres corresponds to the extended chain length, augmented by 0.5 nm to avoid steric repulsion between the end monomers. The NY6 chains were packed in a simple square configuration with a

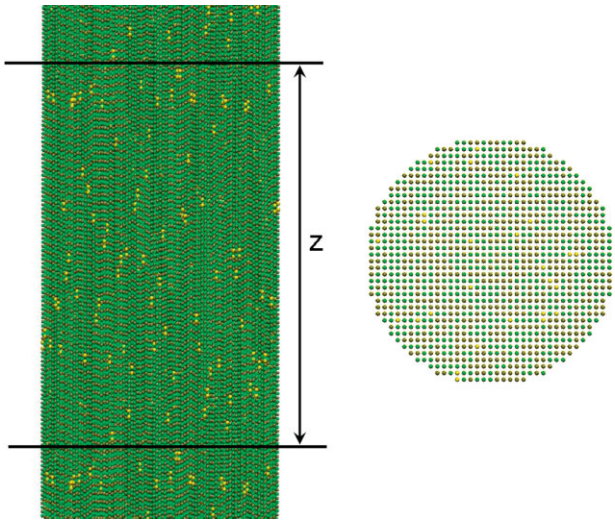

Figure 3. Views of the initial configuration in the simulation of the R10 nanofibre. The inner C1 beads are green, the P4 beads are grey. The terminal C1 beads are yellow, to allow visualization of the random chain displacements along *z*. The nanofibre periodicity ($Z = 32.54$ nm) has been highlighted in the left-hand view. These pictures and those in Figure 4 and 5 have been produced with VMD.[34]

nearest-neighbour distance of 0.53 nm (minimum of LJ potential in the MARTINI FF), and they were given random displacements along the *z*-axis. In this way, we were able to model infinite fibres, without using infinite chains (which, because of the bonding constrains across the simulation cell, could have undergone only minor conformational changes even at high temperatures), and without any discontinuities along the fibre axis (which would have arisen if all the chains had begun and terminated at the same height). Clearly, these systems represent the upper limit to the order and anisotropy that can be expected to occur in an electrospun nanofibre. The other starting configurations, which are completely disordered and isotropic, represent the other extreme. Real systems will reasonably fall somewhere in between.

The nanofibre simulations have been carried out at different temperatures, by application of the Berendsen thermostat with a time constant $\tau_T = 0.1$ ps.[30] Each nanofibre was subjected to a whole heating–cooling cycle. Starting from the ordered configurations described above, we simulated by MD the systems at 300 K. The final structures at 300 K were used as starting points for 400 K simulations, and the last points of the latter as an input to the 500 K simulations. This last step melted the polymer and generated the amorphous nanofibres, which were used as a starting points to repeat the simulations at 300 and 400 K. Accordingly, we shall use the following type of shorthand notation: R7T300KH denotes the simulation of a R7 fibre at 300 K, during the heating cycle (i.e., starting from the ordered chain-extended configuration), R10T400KC denotes the simulation of a R10 fibre at 400 K, during the cooling cycle (i.e., starting from 500 K), R14T500K denotes simulation of a R14 fibre at 500 K (no need to specify H or C in this case). Table 1 provides a summary of all the systems and simulation times.

Table 1. Summary of the systems and overall simulation times, in ns. In all cases, only the last 60 ns were considered for the final data analysis.

	Heating			Cooling	
	300 K	400 K	500 K	400 K	300 K
R7, 553 chains	300	180	120	120	660
R10, 1 109 chains	300	180	120	120	1 300
R14, 2 201 chains	600	420	120	120	720

The CG simulations at 300 and 400 K have been carried out using a time step of 0.02 ps. In the case of simulations at 500 K, a time step of 0.01 ps had to be used in order to obtain stable results (according to our tests, a similar reduction of the time step did not have significant effects of the simulations at lower temperatures). These time steps are short compared to that suggested in the early MARTINI publications.[21] More recently, different authors have also recommended the use of shorter time steps.[31]

Several quantities (average potential energy, density, mean-square displacements of the chains, etc.) were monitored to check proper equilibration of the simulated systems. In some cases, this equilibration required about 1 μs (see Table 1 and Figure S2). Notice that, due to the accelerated dynamics exhibited by CG force fields such as MARTINI, the reported 'simulated time' should be multiplied by a factor of the order of 4–6 to obtain an estimate of the 'real time'.[21] After this equilibration, production runs were typically carried out for another 60 ns. Only this last part of the simulation was analysed, to obtain bead–bead pair distribution functions, mean-square displacements and diffusion constants, end-to-end distances and radii of gyration, density profiles and orientational order parameters. This analysis was carried out with the standard tools implemented in GROMACS or with home-made codes.

Results and Discussion

We begin our discussion with a few qualitative observations, which will be substantiated afterwards by the quantitative analysis of our simulation data. Figure 4–6 contain representative snapshots of the equilibrated systems at different stages of the heating–cooling cycles. All the fibres show a similar evolution. The initial ordered configurations sketched in Figure 3 are largely retained

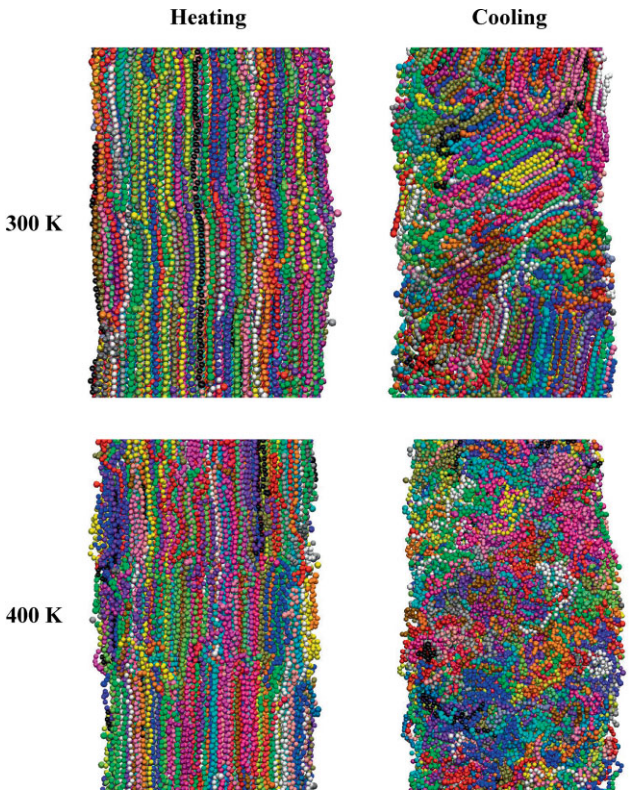

Figure 4. Final snapshots of the 7 nm fibre at different stages of the heating–cooling cycle. The chains have been drawn in different colours so as to highlight their individual states.

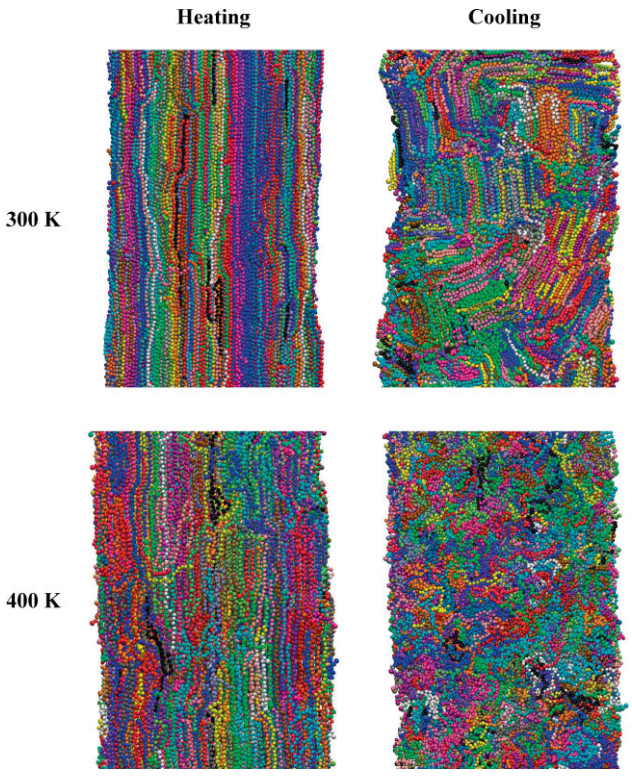

Figure 5. Final snapshots of the 10 nm fibre at different stages of the heating–cooling cycle.

when running the simulation at 300 K. All the chains remain nicely aligned along the fibre axis, but they lose their original square-planar packing to adopt a near-hexagonal one (see Figure S3). The fibre surfaces appear to be quite uniform, sharp and ordered. After raising the temperature to 400 K, the degree of disorder increases slightly and a small fraction of chains shows a deviation from linearity, in the form of chain folding. Apparently, little of significance has occurred, since most chains have retained their straight conformation and their orientation along *z*. However, we shall see that these minor structural perturbations are accompanied by a significant change in the polymer dynamics.

When the temperature is further raised to 500 K, the chains switch to an isotropic random coil conformation, without any apparent preferential orientation. These states are not shown in Figure 4–6, since they look quite similar to those obtained after cooling back to 400 K. Notice that the thinnest nanofibre is no longer perfectly cylindrical. For even thinner fibres, similar shape fluctuations would grow further and eventually lead to the breakup of the fibre into spherical liquid droplets. This shape transformation is driven by a decrease in the exposed surface area and corresponds to the previously mentioned Rayleigh

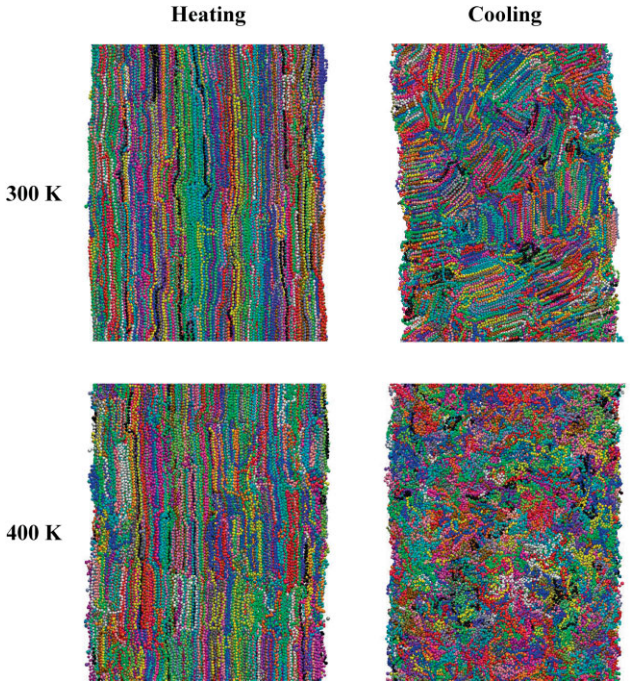

Figure 6. Final snapshots of the 14 nm fibre at different stages of the heating–cooling cycle.

instability. These shape fluctuations can be 'frozen in' upon cooling down to room temperature, leading to nanofibres which have a somewhat jagged interface.

Re-crystallization of the systems finally takes place upon cooling back to 300 K, to give a new state which is clearly different from the original chain-extended one. Now lamellar-like domains are formed by chain-folded molecules. The folds appear to be fairly regular and tight, without long loops between the crystallized segments. Also, there seems to be a fairly well-defined characteristic thickness for the lamellae. The size of the lamellar bundles appears to be comparable with the radius of the thinnest fibre. Finally, these microdomains do not have a well-defined orientation but they are randomly oriented with respect to the fibre axis. This last observation will be confirmed below by the analysis of the orientational order parameters. These observations are significantly different from those of Mattice and coworkers[12c] who, after quenching their PE fibres to room temperature, observed chain-extended crystallization, with the chain axes aligned along the fibres. The detailed investigation of the structure of the lamellae and of the mechanisms leading to their formation will be left for future work.

Our results locate the equilibrium melting temperature of our systems somewhere between 400 and 500 K. Encouragingly, these values are roughly consistent with the experimental result for the NY6 α polymorph (215 °C = 488 K).[17a] However, we have not attempted to pin it down more precisely, for at least a couple of reasons. First of all, this would be a time-consuming and difficult task, due to the first-order nature of the melting and freezing phase transitions. Such transitions proceed by nucleation and growth and therefore may easily exhibit undercooling of the liquid or (not very likely in the present situation, due to the large amount of exposed surfaces) superheating of the solid. Secondly, the MARTINI force field has a general tendency to overestimate the stability of solid phases (for example, 'anti-freeze particles' are required to prevent the crystallization of water at room temperature)[21], so one cannot usually hope to have good agreement for this particular quantity.

We now proceed by presenting a series of computed parameters and observables, so as to extend and provide some formal quantitative support to our qualitative observations. Since different fibres tend to behave similarly in many respects, in many figures we report only the results for the thinnest one (radius = 7 nm). The Supporting Information contains the graphs and data for all the cases. In Figure 7 and S4, the number density profiles of the CG beads are reported as a function of the distance from the fibre centre. These have been calculated by averaging along the full length of the fibres. It can be seen that the densities near the centre of the fibres at 300 and 400 K upon heating are similar and this is consistent with a high degree of

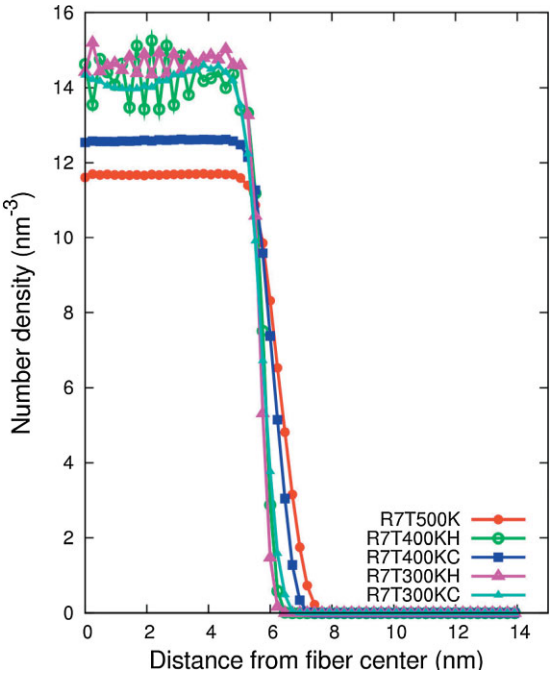

Figure 7. Number density values (beads · nm^{-3}) as a function of the distance from the fibre centre for the nanofibre of radius 7 nm.

crystallinity characterizing these systems. There is a very significant density mismatch between the original and the cooled samples at 400 K, because in the latter case the chains are still in the amorphous state. Instead, the densities return to their original values at 300 K, where chain-folded crystallization occurs.

The bead number densities can be translated into conventional mass densities, using 56.6 g · mol^{-1} for the average mass of a CG bead (half of the mass of a polymer repeat unit). Our upper and lower values of the density are about 1.37 g · cm^{-3} (interior of the nanofibres at 300 K) and 1.09 g · cm^{-3} (interior of the nanofibres at 500 K). These may be compared with the upper and lower experimental values for NY6,[32] which are 1.24 g · cm^{-3} (α crystal phase at room temperature) and 0.96 g · cm^{-3} (polymer melt at 270 °C = 543 K). Thus, our model tends to overestimate the density by 10–13%, depending on the polymer thermodynamic state. This error is not surprising, considering the lack of directional hydrogen bonding and MARTINI's assumption of identical LJ diameters for all conventional particle types.[21] Of course, a better agreement could be obtained by optimizing these LJ parameters, which, however, would break the consistency and transferability from the original model. Notice that a smaller density increase was seen also in the short PEO oligomers (6–8% above experiment), which are somewhat 'easier' than NY6 since they are not hydrogen bonded.[21d]

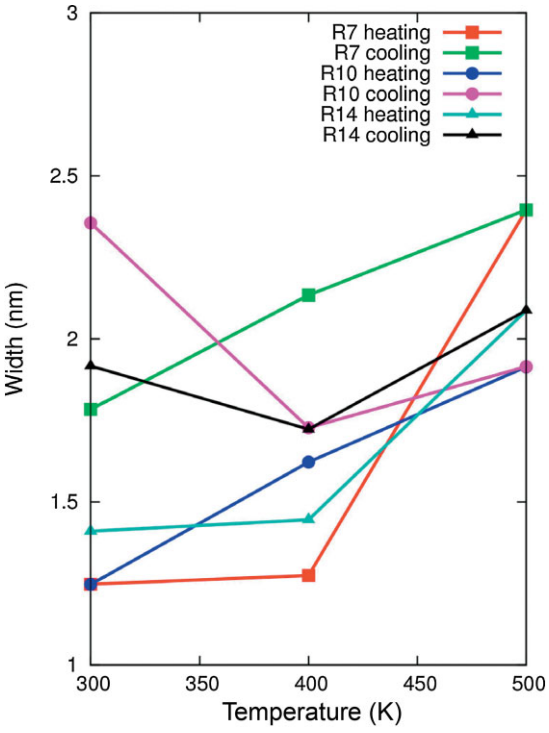

Figure 8. Width of the interfaces showing number densities values ranging between the values of the inner part of the fibre and the vacuum. Values are reported for all the nanofibres here studied for the heating and cooling cycles.

Since the periodicity of the fibres is fixed at the value of the *z* cell axis (32.54 nm in our simulations), a decrease of the polymer density inside the fibres must necessarily be accompanied by an increase of their average diameter and of the thickness of their interface with vacuum. In order to investigate this point, we have extracted the width of the interface by linear fits of the density profiles, in the neighbourhood of the inflection points. The results of this analysis are plotted in Figure 8 for all fibre diameters. As expected, the interface width is largest for the thinnest fibre at the highest temperature. At lower temperatures, we observe a clear difference between the results upon heating and cooling. The latter are always broader than the former. Also, the interface usually becomes sharper at lower temperatures. However, the R10T300KC and R14T300KC samples seem to have a very wide interface, which in the first case is actually larger than at 500 K. In a certain sense, this apparent anomaly depends on the way in which the data were analysed. If we look again at Figure 4–6, we see that the *local* interface widths (i.e., the widths which would have been measured if had considered only one nm-thin slice at a time in the analysis) seem to be roughly comparable in the heating and cooling cycles, and the interface of the R10T300KC sample is locally just as sharp as that of (for example) the R10T300KH one. However, by averaging over the full length of the fibres, we have implicitly mixed short- and long-wavelength fluctuations of the interface. The latter correspond to the surface irregularities, which are 'frozen' in the fibres upon re-crystallization during the cooling stage. Therefore, the broadening in the cooling cycle and the wide interface of the R10T300KC largely reflect the jagged surfaces of the chain-folded fibres.

The local packing order of the polymer units has been characterized by calculation of the different radial distribution functions (RDF's), in this case $g_{C1C1}(r)$, $g_{C1P4}(r)$, $g_{P4P4}(r)$. In Figure 9, we report the RDF's for the 7 nm fibre at different temperatures. As expected, during heating at 300 and 400 K we obtain very structured RDF's with a multiplicity of sharp, regularly spaced peaks. These features are consistent with the extended-chain conformation and crystal-like intermolecular packing (see, however, the discussion of chain diffusion, indicating substantial differences in chain dynamics despite of this structural similarity). When raising the temperature to 500 K, this high degree of order is lost and we only see a few short-range peaks commonly associated with liquid-like packing. Crystal-like order is recovered only by cooling back to 300 K. Here the RDF's have again a comparable but somewhat less perfect degree of structuring, consistently with the chain-folded mode of crystallization.

The RDF's describe the structure of the fibres at the monomer scale, but they do not provide much information about the structure at the scale of the polymer molecules. We already know from Figure 4–6 that these may exist in three possible conformations: extended, random-coil and folded. To characterize them, we have calculated the end-to-end distance and the radius of gyration of the chains. These quantities have been obtained by considering several snapshots of the systems, at different times during the final production runs. The probability distributions of the end-to-end distances are reported in Figure 10 and S5, for each temperature. The persistence of a highly oriented state during heating at 300 and 400 K is demonstrated by the tall and sharp peak in this function at about 26 nm. Instead, when the fibres are heated to 500 K, they melt and the chains turn into a random coil state. The sharp peak at 26 nm is thus replaced by a broad one at about 5 nm. The same distribution is found also at 400 K and, interestingly, it changes very little also after cooling down to 300 K. This means that chain-folded crystallization can occur without major changes in the large-scale conformation and orientation (see below) of the polymer molecules.

The mean-square end-to-end distance of the chains provides a further test of our CG model of NY6. Taking the R14T500K fibre as the system which is closest to the bulk polymer melt, where by Flory's argument the chains should have an unperturbed random-coil conformation, we have $\langle R_{ee}^2 \rangle = 39.6\ \text{nm}^2$. From this we may calculate the char-

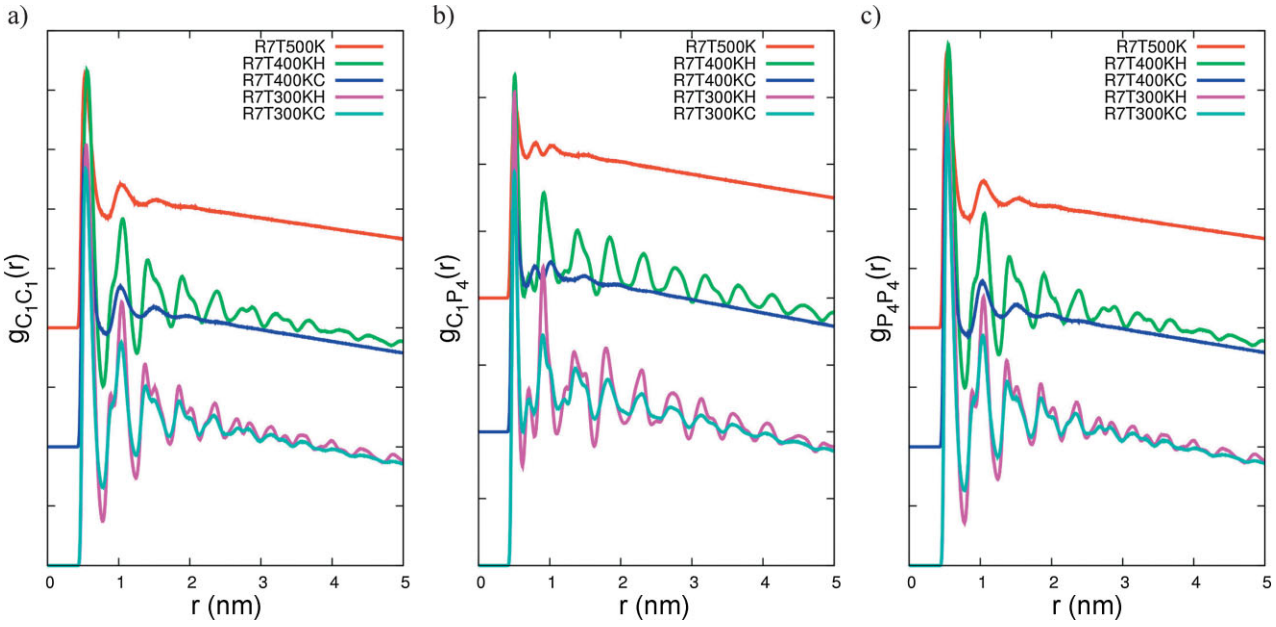

Figure 9. Radial distribution functions computed for the fibre of radius 7 nm at different temperatures: (a) C1–C1, (b) C1–P4, (c) P4–P4. The curves for $T = 400$ K and $T = 500$ K have been shifted upwards for clarity.

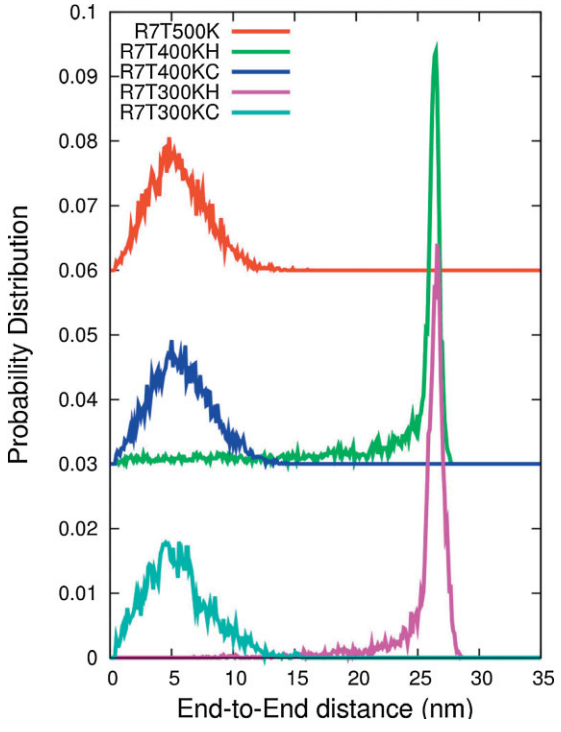

Figure 10. Probability distributions of the chain end-to-end distances, for the nanofibre of radius 7 nm at different temperature. The curves for $T = 400$ K and $T = 500$ K have been shifted upwards for clarity.

acteristic ratio as $C_\infty = \langle R_{ee}^2 \rangle / (nl^2)$, where $n = 318$ is the number of atomistic bonds in a chain and $l = 0.154$ nm is the standard C–C bond length. From this we find $C_\infty = 5.25$, which compares favourably with the experimental values of 5.3 and 6.35.[32] Thus our CG model produces the correct overall stiffness of the NY6 chains.

The probability distributions of the chain radii of gyration are reported in Figure 11 and S6. In order to characterize the possible anisotropy of the chains associated with their confinement within the nanofibres, we have actually produced two separate distributions for the perpendicular and the parallel components, respectively, defined as $S_\perp = \left(S_{xx}^2 + S_{yy}^2\right)^{1/2}$ and $S_{||} = S_{zz}$. Very different values of these components indicate a strong preferential orientation of the chains along the fibre axis and/or a highly anisotropic conformation. As expected, very different components ($S_{||} \gg S_\perp$) are observed for the fibres during heating at 300 and 400 K. The anisotropy virtually disappears upon melting at 500 K and is never recovered, even after re-crystallization at 300 K. Indeed, in the discussion of Figure 4–6, we have already commented that the lamellar domains seem to be randomly oriented with respect to the fibre axis.

We have also calculated the following orientational order parameter, borrowed from the theory of nematic liquid crystals:

$$P_2 = \left\langle \frac{3}{2}\cos^2\vartheta - \frac{1}{2} \right\rangle \quad (3)$$

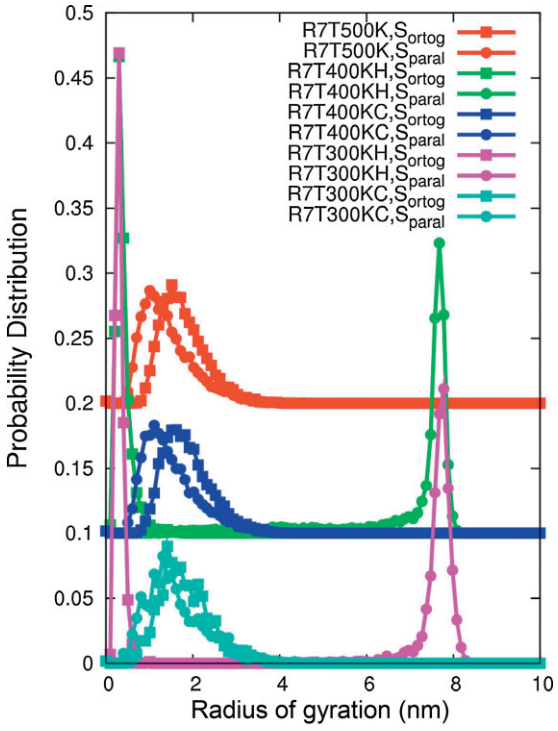

Figure 11. Probability distributions of the radii of gyration (in the orthogonal and parallel directions with respect to the fibre axis, *z*) at the different temperatures and for the nanofibre of 7 nm radius. The curves for $T = 400$ K and $T = 500$ K have been shifted upwards for clarity.

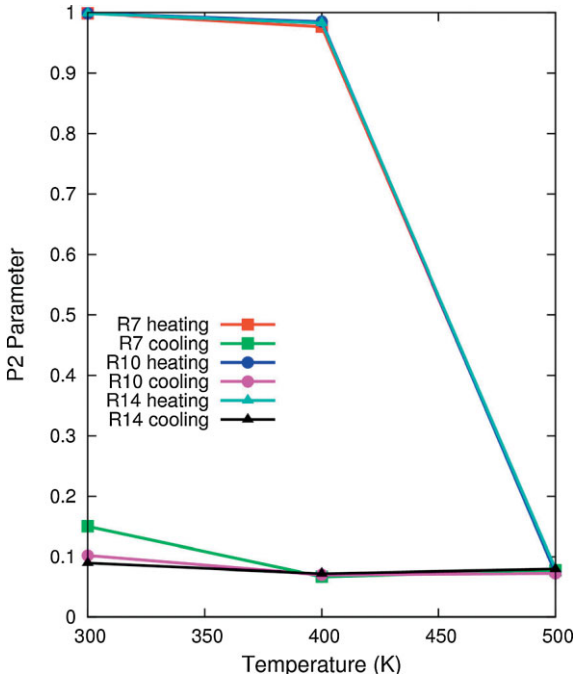

Figure 12. Calculated P_2 orientational order parameters, calculated between the fibre axis and the end-to-end vector of the polymer chains.

Here ϑ is the angle formed by the end-to-end vector of each chain with the *z*-axis, and $\langle \bullet \rangle$ indicates an average over all the chains from several independent configurations of the system, after equilibration. The resulting values of P_2 are plotted as a function of temperature in Figure 12. Once more, we see that the chains are initially well oriented. Their orientation is lost almost completely at 500 K, and it is never recovered on going back to lower temperatures.

Figure 13 shows another P_2 order parameter, which is defined as in Equation (3) except that now ϑ is the angle formed by the individual CG bonds, instead of whole chains. Also, the averages have been restricted to bonds belonging to cylindrical shells and the results have been plotted as a function of their distance from the fibre centre. Thus Figure 13 illustrates the orientational order at a very local scale, unlike Figure 12 which provided a global measure. The most interesting conclusion concerns the structure of the nanofibres at 400 K, in the heating part of the thermal cycle. It can be seen that the orientational order at the fibre centre is virtually identical to the starting one at 300 K, whereas at the fibre surface there is a 1–2 nm thick layer with a much lower orientational order. This agrees with general idea that melting of the nanofibres should start from the surface and then proceed towards their interior.

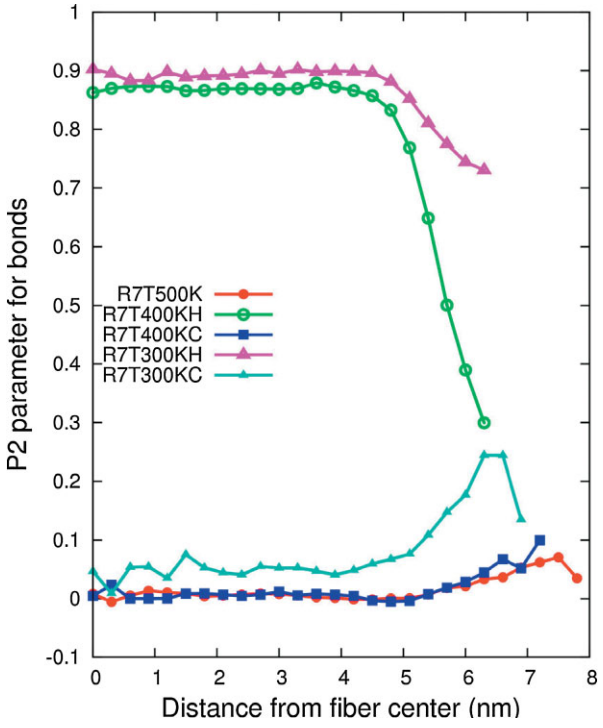

Figure 13. Calculated P_2 orientational order parameters for the bonds, as a function of the distance from the axis for the nanofibre of radius 7 nm.

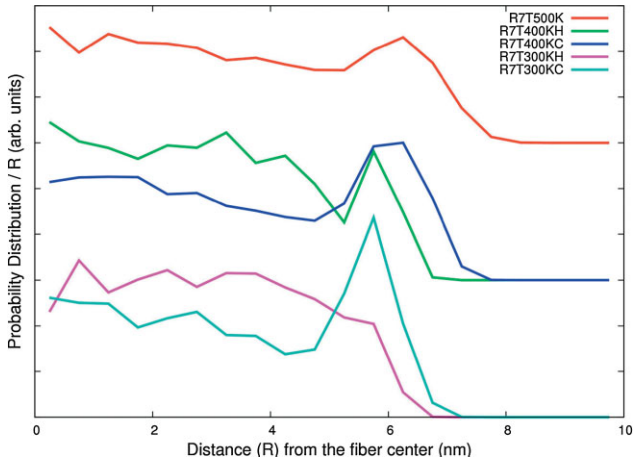

Figure 14. Density of chain ends (arbitrary units), as a function of the distance from the axis for the nanofibre of radius 7 nm. The curves for $T = 400$ K and $T = 500$ K have been shifted upwards for clarity.

The nanofibres at 500 K are everywhere isotropic, and so are those obtained in the cooling part of the thermal cycle. Figure 13 actually indicates a slight orientational order at the surface of the R7 fibre, but these results may well be accidental as it does not seem to occur in the thicker fibres (see Figure S7).

Figure 14 and S8 contain plots of the density of the chain terminals, as a function of the distance from the fibre axis. To obtain them, we have simply counted the number of terminal at a distance R from the axis, and then divided this number by R to take account of the increasing volume of the concentric cylindrical shells. In the initial low-temperature simulations, the terminals are evenly distributed across the fibre but, upon melting at 500 K, they clearly tend to accumulate at the interface. This effect has an entropic origin and is responsible for the molecular weight dependence of the surface tension of polymeric liquids. It has been seen many times in the simulation of polymer–vacuum interfaces, including nanofibres.[12] This terminal-rich interface is retained also when the fibres are cooled back to room temperature. This agrees with our previous observation, that chain-folded crystallization does not require any large-scale changes to the overall chain distribution.

The previous discussion has concerned exclusively the structural properties of the nanofibres. A more complete picture can be obtained by considering also the dynamics of the polymer chains. We do this by briefly discussing the mean-square displacements of the chains along the fibre axis:

$$\mathrm{MSD}_{zz}(t) = \left\langle \left[z_i^{\mathrm{CM}}(t + t_0) - z_i^{\mathrm{CM}}(t_0) \right]^2 \right\rangle \quad (4)$$

where $z_i^{\mathrm{CM}}(t_0)$ is the z-coordinate of the centre-of-mass of chain i at time t, and $\langle \bullet \rangle$ indicates an average over all chains and over different choices of the reference time t_0. The results are plotted in Figure 15. To facilitate comparisons, the plots have been grouped both according to the fibre radius and to the system temperature (see also Figure S5).

Considering first the effect of temperature (left-hand side of Figure 15, for the 7 nm fibre), we observe that the polymer chains do not diffuse at 300 K, both in the original chain-extended state and in the final chain-folded one. This confirms that these states are indeed 'solid'. At 500 K, the chains are fairly free to translate along the fibre axis, despite of their mutual entanglements (which can be reasonably expected to exist, for our chains of 91 CG beads). The most interesting case is probably the one at the intermediate temperature. The diffusive regime with $\mathrm{MSD}_{zz} \propto t$ is reached within the time scale of our simulations, so that both the chain-extended and the random-coil states (from the heating and cooling stages, respectively) can be rightly classified as 'liquid-like'. There is, however, a quantitative difference, since the chains are seen to be more mobile in the disordered phase. This is consistent with the different degrees of structuring in the RDF's characterizing these states (see again Figure 9 and its discussion). We point out that this situation might be reserved for longer polymers, owing to different scaling laws for the chain-length dependence of the diffusion coefficients in the oriented and in the random-coil (i.e., highly entangled) states.

The dependence of the chain diffusion coefficients on fibre radius is also interesting (right-hand side of Figure 15, for $T = 400$ K). All the disordered fibres from the cooling part of the cycle are characterized by the same chain diffusion coefficients. Instead, there is a strong dependence on the radius for the oriented fibres, in the heating part of the cycle. The chains in the thinnest fibre are much more mobile than those in thicker ones. Most likely, this is the result of different chain dynamics at the interior and exterior of the fibres, in analogy with the findings by Rutledge and co-workers[13] in their MD simulations of glassy nanofibres.

Summary and Conclusion

We have described the implementation of a CG force field for the simulation of nylon-6 (NY6). Our model is based on the MARTINI parametrization for the non-bonded interactions and on Boltzmann-inverted atomistic simulations for the bonded ones. We have then applied the CG model to the simulation of electrospun nanofibres with diameters and polymer chain lengths approaching realistic values. The fibres are effectively infinite and isolated, being surrounded

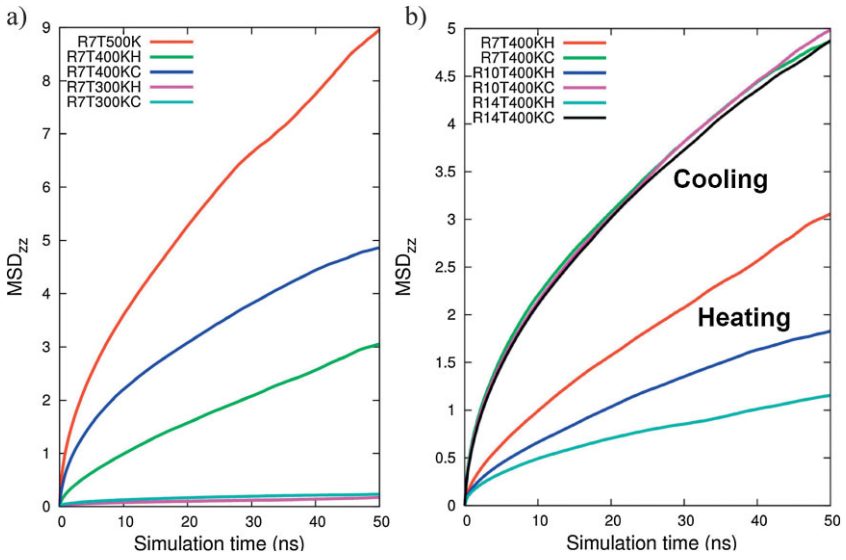

Figure 15. Plots of the *zz* component of the mean-square displacements of the chains: (a) Comparisons at different temperatures, for the fibre of radius 7 nm; (b) comparisons for fibres of different radii (7, 10 and 14 nm) at 400 K.

by vacuum. The description obtained from the simulations appears to be consistent with behaviour observed experimentally for NY6 nanofibres,[15,16] thus demonstrating that this CG approach can be used as an interpretative tool to investigate the interplay of structure and properties in these systems.

It is an experimental fact that the structure and properties of electrospun nanofibres depend crucially on processing conditions and post-processing treatments. In other words, these fibres may exist in one or another metastable state, depending on their previous history.[15] Similarly, in our simulations the nanofibre structure depends markedly on the thermal history (from 300 to 500 K and back). At room temperature, the polymer chains are crystallized either in a chain-extended or in a chain-folded state. At a higher temperature, they may be in a nematic liquid-crystalline state or in an undercooled amorphous state. Finally, at an even higher temperature, they are found in a molten state. In connection with this, we notice that the transition from a chain-extended (γ crystal phase) into a chain-folded state (α crystal phase) has also been observed experimentally for NY6 nanofibres.[15b] We also point out that chain-folded crystallization did not occur in the previous simulations of PE nanofibres.[12,13] Instead, upon cooling from the isotropic melt state, the Mattice group observed chain-extended crystallization and formation of nearly single-crystal-like nanofibres[12c] (as in the initial, low temperature state of our simulations). This qualitative difference between their and our own results might be due the different polymer models (on-lattice PE vs. off-lattice NY6), but more likely it originates from the different simulation methods. In fact, the MC simulations[12] alternated local single-bead and collective multi-bead pivot moves. The latter, which have no equivalent in MD, were adopted because of their demonstrated effectiveness in overcoming kinetic barriers and ensure full attainment of the true equilibrium state. This is clearly an advantage from the point of simulation efficiency. However, one should also bear in mind that such kinetic barrier do exist in real polymer systems, and any method which adopts some artificial dynamics so as to overcome them might fail to reproduce some relevant experimental observations.

Apparently, and somewhat unexpectedly, in most cases the nanofibre diameter (14, 20 or 28 nm) does not seem to have a major impact on the internal structure and dynamics of the polymer chains. All the nanofibres have the same qualitative behaviour with respect to thermal history. The interfacial thickness, the chain conformation (end-to-end distance and radius of gyration), the local chain packing (radial distribution functions) and orientation (P_2 order parameter) are all very similar. Presumably, it would be necessary to go to even thinner fibres so as to see a substantial change in these properties. Or, perhaps, a stronger dependence on fibre radius could be seen in systems with more weakly interacting chains. In fact, both of these condition were met in the PE nanofibre simulations by Rutledge and co-workers.[13] If, on the other hand, we stick to a hydrogen bonded polymer such as NY6, we might observe a stronger size dependence on going to an aqueous medium. In this case, water may penetrate the fibres and displace some amide groups from their hydrogen bonding interactions, thus weakening the polymer–polymer interactions. We are planning to investigate this situation in the future.

The present work may evolve along several different directions. First of all, we plan to improve and extend our CG parametrization for NY6 and other polymers relevant for biomedical applications of electrospun nanofibres, such as polyesters. Another possibility, which has just been mentioned, is the study of different polymer systems and of the interaction of the fibres with the environment (aqueous solutions and organic solvents, as well as proteins and polypeptides). We would also like to investigate more thoroughly the consequences of the different types of structural organization of the polymer chains, by establishing a closer connection with experimentally relevant properties. For example, if we limit ourselves to the crystalline systems, we expect that the fibres with chain-

extended crystallization should have superior mechanical properties. Instead, the fibres with lamellar chain-folded crystallization should have better absorption properties, due to their jagged interface. The simulation of mechanical stretching of the amorphous or chain-folded nanofibres would also be interesting as mean to produce new starting states characterized by a partial degree of anisotropy. Finally, it should be interesting to analyse in greater detail the phenomena occurring during the fusion and re-crystallization of the polymer chains.[33] At a fundamental level, these electrospun nanofibres represent a beautiful model system for the study of polymer phase transitions in confined, low-dimensional systems.

Acknowledgements: We thank Chiara Bertarelli, Andrea Bianco and Stefano Valdo Meille for several discussions on the electrospinning technique and the polyamide crystal structures. We also thank Luca Monticelli and Siewert-Jan Marrink for useful correspondence about the MARTINI approach, at the beginning of this work.

Received: January 27, 2011; Revised: March 30, 2011; Published online: May 20, 2011; DOI: 10.1002/mats.201100010

Keywords: coarse-graining; crystallization; electrospinning; molecular dynamics; nylon

[1] E. P. Giannelis, R. Krishnamoorti, E. Manias, *Adv. Polym. Sci.* **1999**, *138*, 107.
[2] [2a] A. C. Balazs, T. Emrick, T. P. Russell, *Science* **2006**, *314*, 1107; [2b] R. A. Vaia, J. F. Maguire, *Chem. Mater.* **2007**, *19*, 2736; [2c] J. Jancar, J. F. Douglas, F. W. Starr, S. K. Kumar, P. Cassagnau, A. J. Lesser, S. S. Sternstein, M. J. Buehler, *Polymer* **2010**, *51*, 3321.
[3] [3a] G. Allegra, G. Raos, M. Vacatello, *Prog. Polym. Sci.* **2008**, *33*, 683; [3b] T. A. Vilgis, G. Heinrich, M. Klüppel, Reinforcement of Polymer Nanocomposites: Theory, *Experiments and Applications*, Cambridge University Press, Cambridge **2009**.
[4] [4a] S. Günes, H. Neugebauer, N. S. Sariciftci, *Chem. Rev.* **2007**, *107*, 1324; [4b] B. C. Thompson, J.-M. Frechet, *Angew. Chem., Int. Ed.* **2008**, *47*, 58.
[5] P. Rittigstein, R. D. Priestley, L. J. Broadbelt, J. M. Torkelson, *Nature Mater.* **2007**, *6*, 278.
[6] [6a] D. M. Lincoln, R. A. Vaia, Z. G. Wang, B. S. Hsiao, R. Krishnamoorti, *Polymer* **2001**, *42*, 9975; [6b] E. Manias, A. Touny, L. Wu, K. Strawhecker, B. Lu, T. C. Chung, *Chem. Mater.* **2001**, *13*, 3516; [6c] A. Famulari, P. Arosio, S. Filippi, C. Marazzato, P. Magagnini, L. Minkova, S. V. Meille, *J. Macromol. Sci. B* **2007**, *46*, 355.
[7] [7a] A. Tuteja, M. E. Mackay, S. Narayanan, S. Asokan, M. S. Wong, *Nano Lett.* **2007**, *7*, 1276; [7b] A. Tuteja, P. M. Duxbury, M. E. Mackay, *Macromolecules* **2007**, *40*, 9427.
[8] [8a] D. Li, Y. Xia, *Adv. Mater.* **2004**, *16*, 1151; [8b] A. Greiner, J. H. Wendorff, *Angew. Chem., Int. Ed.* **2007**, *46*, 5670.
[9] G. C. Rutledge, S. V. Fridrikh, *Adv. Drug. Del. Rev.* **2007**, *59*, 1384.
[10] D. H. Reneker, A. L. Yarin, *Polymer* **2008**, *49*, 2387.
[11] [11a] R. Inai, M. Kotaki, S. Ramakrishna, *Nanotechnology* **2005**, *16*, 208; [11b] E. Zussman, M. Burman, A. L. Yarin, R. Khalfin, Y. Cohen, *J. Polym. Sci. B: Polym. Phys.* **2006**, *44*, 1482; [11c] S.-C. Wong, A. Baji, S. Leng, *Polymer* **2008**, *49*, 4713.
[12] [12a] V. Vao-soongnern, P. Doruker, W. L. Mattice, *Macromol. Theory Simul.* **2000**, *9*, 1; [12b] V. Vao-soongnern, W. L. Mattice, *Langmuir* **2000**, *16*, 6757; [12c] G. Xu, V. Vao-soongnern, W. L. Mattice, *Macromol. Theory Simul.* **2002**, *11*, 494.
[13] [13a] S. Curgul, K. J. Van Vliet, G. C. Rutledge, *Macromolecules* **2007**, *40*, 8483; [13b] S. Buell, K. J. Van Vliet, G. C. Rutledge, *Macromolecules* **2009**, *42*, 4887.
[14] [14a] J. L. Keddie, R. A. L. Jones, R. A. Cory, *Europhys. Lett.* **1994**, *27*, 59; [14b] C. J. Ellison, J. M. Torkelson, *Nature Mater.* **2003**, *2*, 695; [14c] M. Alcoutlabi, G. B. McKenna, *J. Phys. Cond. Matter* **2005**, *17*, R461.
[15] [15a] J. S. Stephens, D. B. Chase, J. F. Rabolt, *Macromolecules* **2004**, *37*, 877; [15b] Y. Liu, L. Cui, F. Guan, Y. Gao, N. E. Hedin, L. Zhu, H. Fong, *Macromolecules* **2007**, *40*, 6283; [15c] A. Bianco, G. Iardino, A. Manuelli, C. Bertarelli, G. Zerbi, *Chem. Phys. Chem.* **2007**, *8*, 510; [15d] A. Bianco, G. Iardino, C. Bertarelli, L. Miozzo, A. Papagni, G. Zerbi, *Appl. Surf. Sci.* **2007**, *253*, 8360; [15e] R. Dersch, T. Liu, A. K. Schape, A. Greiner, J. H. Wendorff, *J. Polym. Sci. A* **2003**, *41*, 545.
[16] [16a] L. Li, L. M. Bellan, H. G. Craighead, M. Frey, *Polymer* **2006**, *47*, 6208; [16b] G.-M. Kim, G. H. Micheler, F. Ania, F. J. Balta Calleja, *Polymer* **2007**, *48*, 4814; [16c] Q. Li, D. Gao, Q. Wei, M. Ge, W. Liu, L. Wang, K. Hu, *J. Appl. Polym. Sci.* **2010**, *117*, 1572.
[17] [17a] D. R. Holmes, C. W. Bunn, D. J. Smith, *J. Polym. Sci.* **1955**, *17*, 159; [17b] H. Arimoto, M. Ishibashi, M. Hirai, Y. Chatani, *J. Polym. Sci. A* **1965**, *3*, 317; [17c] P. Simon, G. Argay, *J. Polym. Sci. : Polym. Phys.* **1978**, *16*, 935; [17d] V. Malta, G. Cojazzi, A. Fichera, D. Ajò, R. Zannetti, *Eur. Polym. J.* **1979**, *15*, 765; [17e] K. Miyasaka, T. Isomoto, H. Koganeya, K. Uehara, K. Ishikawa, *J. Polym. Sci. : Polym. Phys.* **1980**, *18*, 1047; [17f] D. R. Salem, H.-D. Weigmann, *Polym. Commun.* **1989**, *30*, 336; [17g] N. S. Murthy, H. Minor, *Polym. Commun.* **1991**, *32*, 297; [17h] N. S. Murthy, *Polym. Commun.* **1991**, *32*, 301; [17i] C. Ramesh, E. Bhoje Gowd, *Macromolecules* **2001**, *34*, 3308; [17j] S. J. Cooper, E. D. T. Atkins, M. J. Hill, *Polymer* **2002**, *43*, 891.
[18] [18a] S. León, C. Alemán, S. Muñoz-Guerra, *Macromolecules* **2000**, *33*, 5754; [18b] Y. Li, W. A. Goddard, *Macromolecules* **2002**, *35*, 8440; [18c] C. Alemán, C. Casanovas, *Colloid Polym. Sci.* **2004**, *282*, 535.
[19] [19a] J. Baschnagel, K. Binder, P. Doruker, A. A. Gusev, O. Hahn, K. Kremer, W. L. Mattice, F. Müller-Plathe, M. Murat, W. Paul, S. Santos, U. W. Suter, V. Tries, *Adv. Polym. Sci.* **2000**, *152*, 41; [19b] F. Müller-Plathe, *ChemPhysChem* **2002**, *3*, 754; [19c] A. P. Lyubartsev, A. Laaksonen, *Lect. Notes Phys.* **2004**, *640*, 219; [19d] S. Izvekov, G. A. Voth, *J. Chem. Phys.* **2005**, *123*, 134105.
[20] H. A. Karimi-Varzaneh, P. Carbone, F. Müller-Plathe, *J. Chem. Phys.* **2008**, *129*, 154904.
[21] [21a] S.-J. Marrink, H. J. Risselada, S. Yefimov, D. P. Tieleman, A. H. de Vries, *J. Phys. Chem. B* **2007**, *111*, 7812; [21b] L. Monticelli, S. K. Kandasamy, X. Periole, R. G. Larson, D. P. Tieleman, S.-J. Marrink, *J. Chem. Theory Comput.* **2008**, *4*, 819; [21c] C. A. Lopez, A. J. Rzepiela, A. H. De Vries, L. Dijkhuizen, P. H. Hunenberger, S.-J. Marrink, *J. Chem. Theory Comput.* **2009**, *5*, 3195; [21d] H. Lee, A. H. De Vries, S.-J. Marrink, R. W. Pastor, *J. Phys. Chem. B* **2009**, *113*, 13186; [21e] G. Rossi,

L. Monticelli, S. R. Puisto, I. Vattulainen, T. Ala-Nissila, *Soft Matter* **2011**, *7*, 698.
[22] [22a] D. van der Spoel, E. Lindahl, B. Hess, G. Groenhof, A. E. Mark, H. J. C. Berendsen, *J. Comput. Chem.* **2005**, *26*, 1701; [22b] B. Hess, C. Kutzner, D. van der Spoel, E. Lindhal, *J. Chem. Theory Comput.* **2008**, *4*, 435.
[23] A P5-type particle would be appropriate for a free Glycine in water, which is found in the zwitterion state. When the same amino acid belongs to a protein or peptide chain, it has no charged groups and so it is represented by a less polar P4-type particle, as we have done in our simulations.
[24] J. W. Ponder, D. A. Case, *Adv. Protein Chem.* **2003**, *66*, 27.
[25] J. W. Ponder, *TINKER: Software Tools for Molecular Design*, 4.2 ed. Washington University School of Medicine, Saint Louis, MO **2004**.
[26] [26a] W. L. Jorgensen, D. S. Maxwell, J. Tirado-Rives, *J. Am. Chem. Soc.* **1996**, *118*, 11225; [26b] G. A. Kaminski, R. Friesner, J. Tirado-Rives, W. L. Jorgensen, *J. Phys. Chem. B* **2001**, *105*, 6474.
[27] Some authors prefer to conduct these atomistic simulations in a condensed phase [typically, the melt state or an aqueous solution]. Gas-phase simulations have been consistently adopted by the Kremer group. See, for example, their recent work on polystyrene: D. Fritz, V. A. Harmandaris, K. Kremer, N. F. A. van der Vegt, *Macromolecules* **2009**, *42*, 7579.
[28] This directionality depends on the orientation of the peptide bonds and it exists also in proteins. It determines, for example, the distinction between parallel and anti-parallel β sheets. Also in this case, the replacement of the atomistic representation [e.g., $-(NH-CH_2-CO)_n-$ for polyglycine] by a coarse-grained one [e.g., $-(P4)_n-$] implies the loss of information on this directionality.
[29] Remember that, after all, it is the bulk state (crystalline, amorphous or other] and not the nanofibres which represents to the true equilibrium state of the polymer!
[30] H. J. C. Berendsen, J. P. M. Postma, W. van Gunsteren, A. DiNola, J. R. Haak, *J. Chem. Phys.* **1984**, *81*, 3684.
[31] [31a] M. Winger, D. Trzesniak, R. Baron, W. F. van Gunsteren, *Phys. Chem. Chem. Phys.* **2009**, *11*, 1934; [31b] S. J. Marrink, X. Periole, D. P. Tieleman, A. H. De Vries, *Phys. Chem. Chem. Phys.* **2010**, *12*, 2254.
[32] J. Brandrup,, E. H. Immergut, (Eds.), *Polymer Handbook*, 3rd edition, John Wiley and Sons, New York, **1989**.
[33] M. Muthukumar, *Lect. Notes Phys.* **2007**, *714*, 1.
[34] W. Humphrey, A. Dalke, K. Schulten, *J. Mol. Graph.* **1996**, *14*, 33.